Electronic Supporting Information

Facile synthesis of one-dimensional $LiNi_{0.8}Co_{0.15}Al_{0.05}O_2$ microrods as advanced cathode materials for lithium ion batteries

Naiteng Wu, Hao Wu*, Wei Yuan, Shengjie Liu, Jinyu Liao and Yun Zhang*

Department of Advanced Energy Materials, College of Materials Science and Engineering, Sichuan University, Chengdu 610065, P. R. China

* Corresponding Author. E-mail: hao.wu@scu.edu.cn and y_zhang@scu.edu.cn

Part I: Experimental Section

Material Synthesis

In this work, all the reagents were analytical grade without further purification and purchased from Chengdu Kelong Chemical Reagents Corporation.

Preparation of $MC_2O_4{\cdot}2H_2O$ (M=Ni, Co, Al) Microrods. $MC_2O_4{\cdot}2H_2O$ microrod precursors were prepared by using a two-step co-precipitation method. Typically, 2.25 mmol of $CoSO_4{\cdot}7H_2O$ was first dissolved in 25 mL of aqueous solution to form a solution, signed as A. Then, 24 mmol of $NiSO_4{\cdot}6H_2O$, 4.5 mmol of $CoSO_4{\cdot}7H_2O$ and 0.75 mmol of $Al_2(SO_4)_3{\cdot}18H_2O$ were together dissolved in 75 mL of aqueous solution to form another mixture solution, signed as B. After that, solution of A was slowly added to 120 mL of $H_2C_2O_4$ solution (0.3 mol/L) under vigorous stirring at room temperature till a $CoC_2O_4{\cdot}2H_2O$-containing suspension was obtained, in which the solution B was then added drop by drop to further get a mixed suspension. After continued stirring for 2 h, the mixed suspension was filtered, washed and finally dried at 80 °C overnight to obtain the $MC_2O_4{\cdot}2H_2O$ microrod precursor.

Synthesis of $LiNi_{0.8}Co_{0.15}Al_{0.05}O_2$ Microrods. $LiNi_{0.8}Co_{0.15}Al_{0.05}O_2$ microrods were synthesized by solid-state reaction between $LiOH{\cdot}H_2O$ and $MC_2O_4{\cdot}2H_2O$ precursor. Typically, the as-

obtained $MC_2O_4 \cdot 2H_2O$ precursor was mixed thoroughly with excess $LiOH \cdot H_2O$ in a molar ratio of 1: 1.02. The mixture was first heated at 500 °C for 5 h, and then sintered at 780 °C for 15 h in pure O_2 atmosphere to obtain the final $LiNi_{0.8}Co_{0.15}Al_{0.05}O_2$ product.

Synthesis of $LiNi_{0.8}Co_{0.15}Al_{0.05}O_2$ Microspheres. For comparison, $LiNi_{0.8}Co_{0.15}Al_{0.05}O_2$ microspheres was also synthesized by using commercial spherical $Ni_{0.8}Co_{0.15}Al_{0.05}(OH)_2$ as precursor (purchased from Ningxia Orient Tantalum Industry Co., Ltd). The commercial $Ni_{0.8}Co_{0.15}Al_{0.05}(OH)_2$ precursor was commonly prepared by a co-precipitation method with $NiSO_4$, $CoSO_4$ and $Al(OH)_3$ as starting materials, ammonia as chelating agent, and NaOH as precipitation agent. For the synthesis of $LiNi_{0.8}Co_{0.15}Al_{0.05}O_2$ microspheres, the $Ni_{0.8}Co_{0.15}Al_{0.05}(OH)_2$ precursor was reacted with $LiOH \cdot H_2O$ by sintering treatment in the same procedure as described in the synthesis of $LiNi_{0.8}Co_{0.15}Al_{0.05}O_2$ microrods.

Characterization

Crystal structures of all samples were identified by X-ray diffraction (XRD, Bruker DX-1000 diffractometer with Cu Kα radiation) in the 2θ angular range of 10-80° at a scanning rate of 0.02°/s. The chemical compositions of the as-prepared samples were analyzed by inductive coupled plasma atomic emission spectrometry (ICP-AES). X-ray photoelectron spectroscopy (XPS, AXIS Ultra DLD, Kratos) was used to characterize valence state of surface elements in products. N_2 adsorption measurements were performed with Tristar 3020 instrument (Micromeritics) to determine the specific surface area of samples. The morphology and element composition of the obtained powders were observed by using scanning electron microscope (SEM, Hitachi S-4800) equipped with energy dispersive spectroscope (EDS). Transmission electron microscope (TEM, JEOL JEM-2100F) and high resolution transmission electron microscope (HRTEM, JEOL JEM-2100F) with an accelerating voltage of 200 kV were used for morphology and structure analysis.

Electrochemical Measurements

The working electrodes were fabricated by dispersing 80 wt. % $LiNi_{0.8}Co_{0.15}Al_{0.05}O_2$ powders (active materials), 10 wt. % carbon black (conductive agent), and 10 wt. % polyvinylidene fluoride (PVDF, binder) inN-methyl-2-pyrrolidone (NMP) solvent to form a homogeneous

slurry, followed by plastering the slurry onto aluminum foil current collector and dried at 120 ºC overnight in a vacuum oven. All electrodes were cut into disks with a diameter of 1.4 cm, the average mass loading of which was about 2.0 mg/cm^2. For electrochemical measurements, CR-2032 coin-type cells were assembled in an argon-filled glove box by utilizing the above prepared pole pieces as cathodes, metal lithium foils as anodes, polypropylene micro-porous films (Celgard 2400) as separators, and 1.0 mol/L $LiPF_6$ dissolved in a mixture of ethylene carbonate (EC) and dimethyl carbonate (DMC) and diethyl carbonate (DEC) (1:1:1 in volume) as electrolyte. The galvanostatic charge and discharge tests of the cells were performed on a Neware program-control test system (Shen Zhen, CT-3008W) in the potential range between 2.7 and 4.3 versus Li/Li^+ at different current densities from 0.1 C (1C=180 mAh/g) to 10 C. The entire charge-discharge tests were carried out at room temperature and 55 ^{o}C. The electrochemical impedance spectra (EIS) of the cells after 100 cycles were carried out in the frequency range from 100 kHz to 10 mHz with an AC amplitude of 5 mV using VMP3 (SN 0746).

Part II: Supporting Figures and Tables

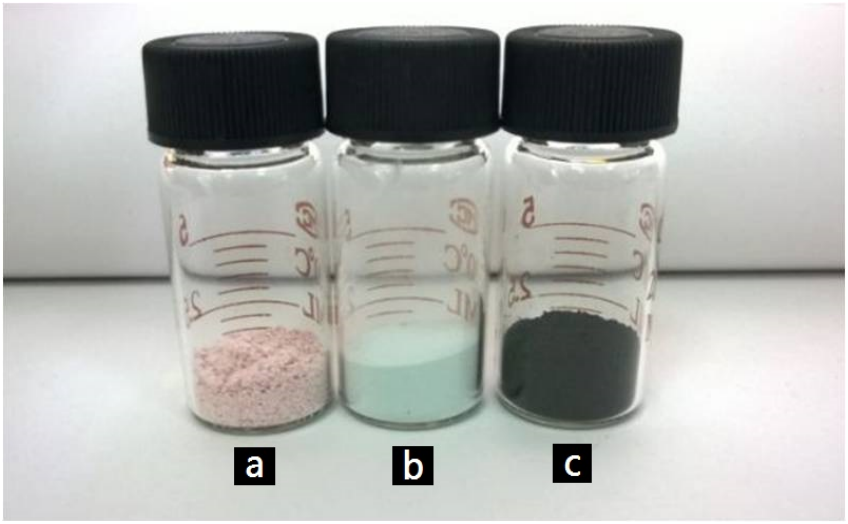

Fig. S1 Photograph of the as-synthesized (a) $CoC_2O_4 \cdot 2H_2O$, (b) $MC_2O_4 \cdot 2H_2O$ precursor, and (d) NCA-MRs product

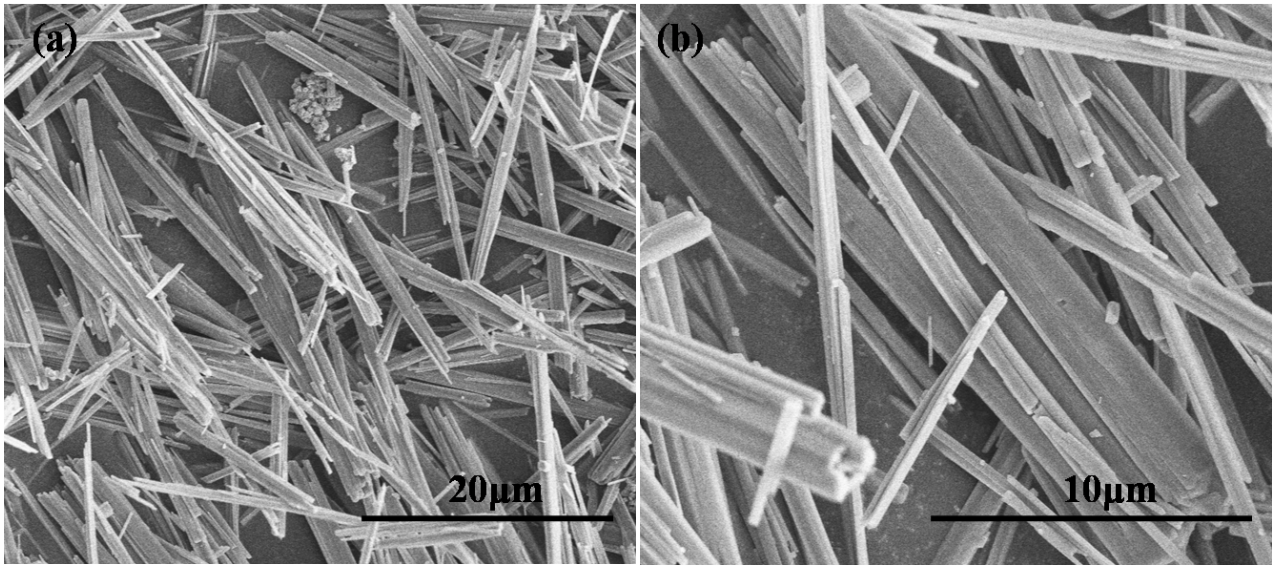

Fig. S2 SEM images of the as-synthesized $CoC_2O_4 \cdot 2H_2O$

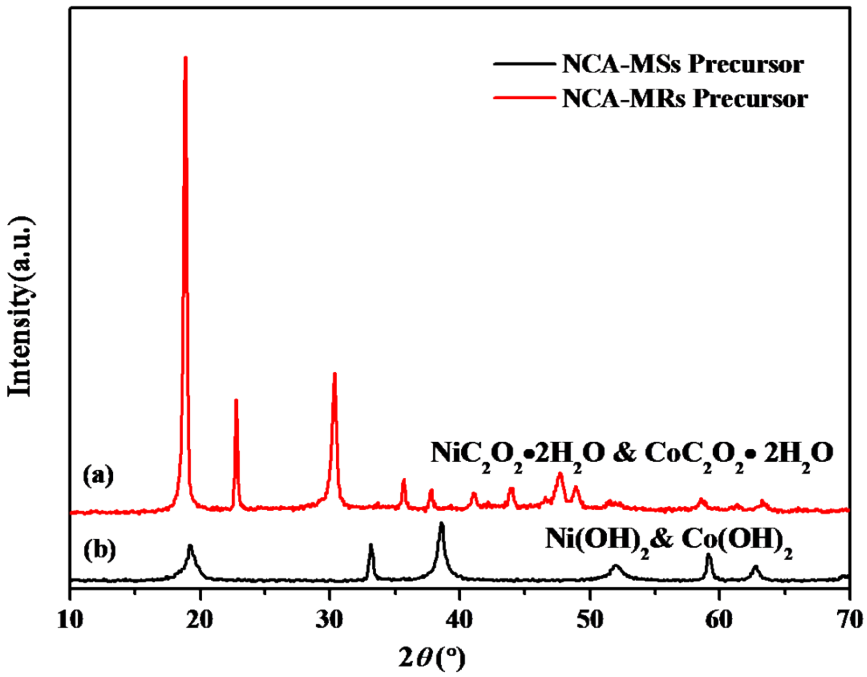

Fig. S3 XRD patterns of the as-obtained precursors: (a) $MC_2O_4 \cdot 2H_2O$, and (b) $Ni_{0.8}Co_{0.15}Al_{0.05}(OH)_2$

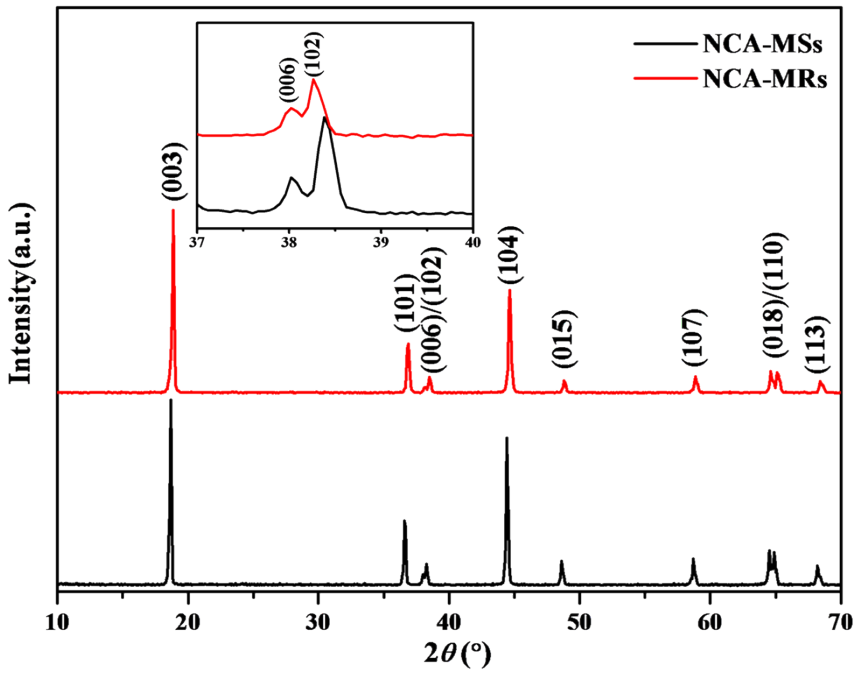

Fig. S4 XRD patterns of the products: (a) NCA-MRs and (b) NCA-MSs, (inset: diffraction peaks of the region from 37 to 40°)

Table S1 Crystal lattice parameters, R-factor and peak ratio of (003)/(104) for NCA-MRs and NCA-MSs calculated from XRD date

Samples	*a*(Å)	*c*(Å)	*c/a*	$I_{(003)}/I_{(104)}$	*R-factor*
NCA-MSs	2.8793	14.0822	4.8907	1.36	0.469
NCA-MRs	2.8629	14.1273	4.9344	1.41	0.443

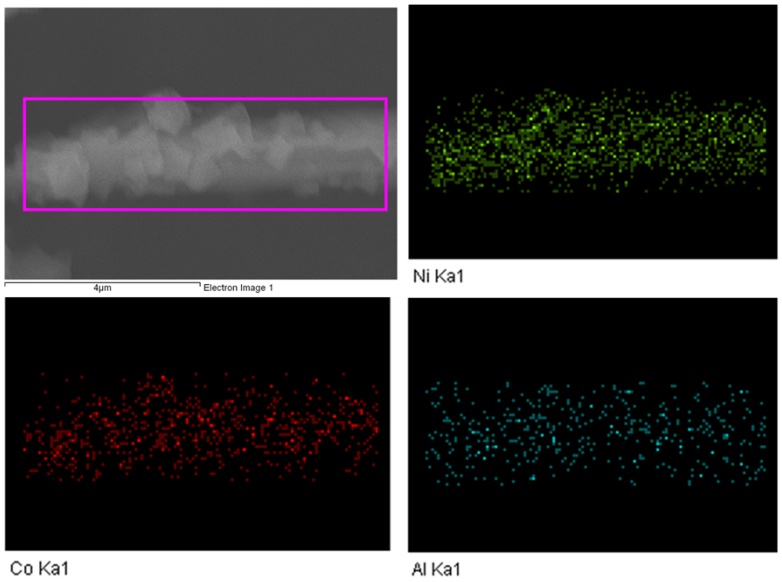

Fig. S5 EDS dot-mapping of Ni, Co, Al elements of $MC_2O_4{\cdot}2H_2O$ precursor

Table S2 Element molar ratios of Li/Ni/Co/Al for the $MC_2O_4{\cdot}2H_2O$ precursor and NCA-MRs product from ICP-AES

Element		Li	Ni	Co	Al
$MC_2O_4{\cdot}2H_2O$ precursor	Content(ppm)		20.54	3.8463	0.7544
	Molar ratio		0.8	0.1492	0.0639
NCA-MRs	Content(ppm)	0.6496	4.352	0.8001	0.1625
	Molar ratio	1	0.7922	0.145	0.0643

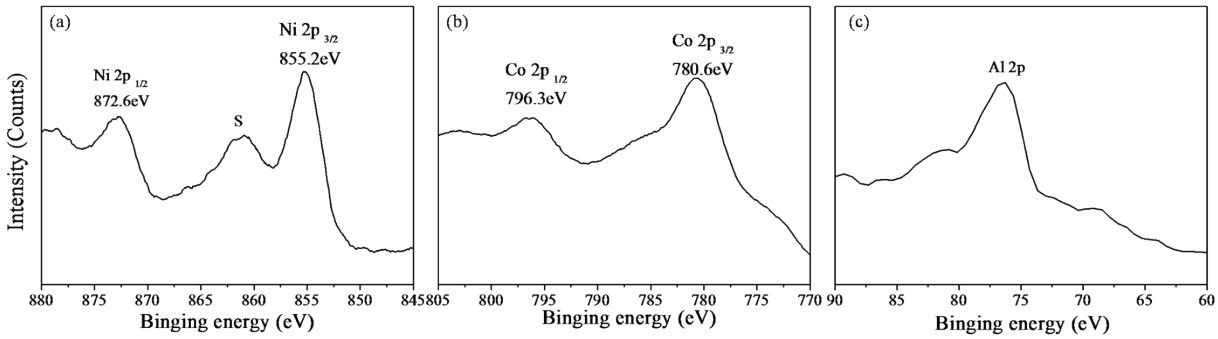

Fig. S6 XPS spectra for (a) Ni, (b) Co, and (c) Al elements of NCA-MRs product. Symbol "S" represents the satellite peaks for Ni 2p levels.[S1]

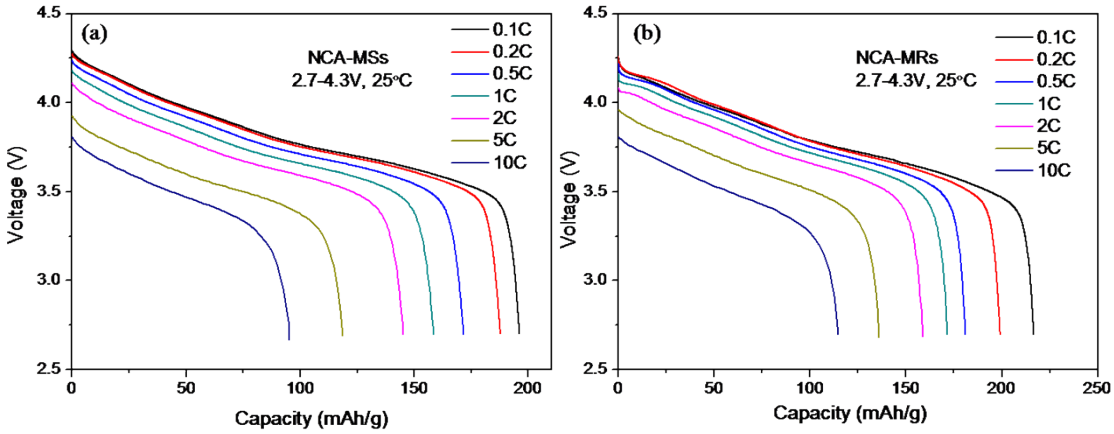

Fig. S7 Typical discharge voltage-capacity profiles of (a) NCA-MSs, (b) NCA-MRs at variable current rate of 0.1, 0.2, 0.5, 1, 2, 5 and 10 C

Table S3 Discharge capacity of the products at variable current rate

Samples	Discharge capacity (mA h/g)							
	0.1 C	0.2 C	0.5 C	1 C	2 C	5 C	10 C	Back to 0.1 C
NCA-MSs	195.2	187.7	171.6	158.4	145.2	118.6	95.1	188.5
NCA-MRs	218.7	200.2	181.1	172.3	159.1	137.4	115.6	214.7

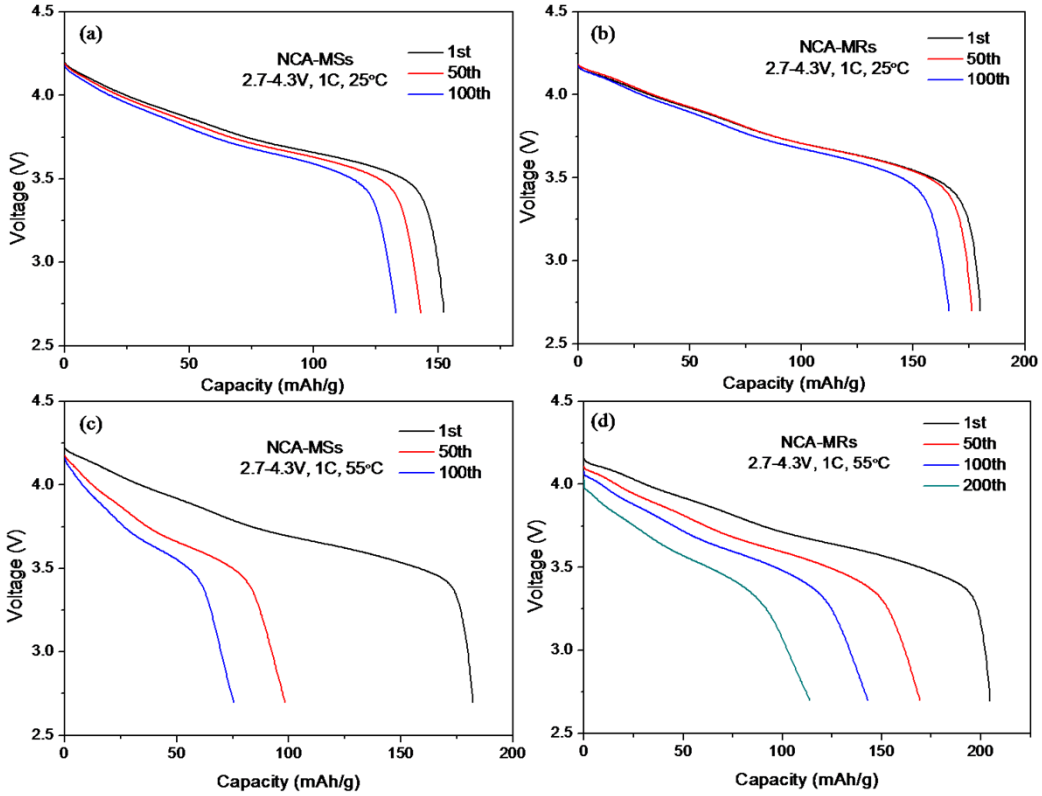

Fig. S8 Typical discharge voltage-capacity profiles of NCA-MSs (a and c) and NCA-MRs (b and d) at the different cycle numbers under 25 (a and b) and 55 °C (c and d)

Table S4. Capacity retention of the products after cycling at 1 C under 25 and 55 °C

	25 °C		55 °C	
	NCA-MSs	NCA-MRs	NCA-MSs	NCA-MRs
Initial capacity (mA h/g)	152.2	180.1	182.4	204.2
The 100th capacity (mA h/g)	132.9	168.2	75.3	147.6
The 200th capacity (mA h/g)				116.7
Final capacity retention (%)	87.3	93.4	41.2	72.3 (100 cycles)/ 57.1 (200 cycles)

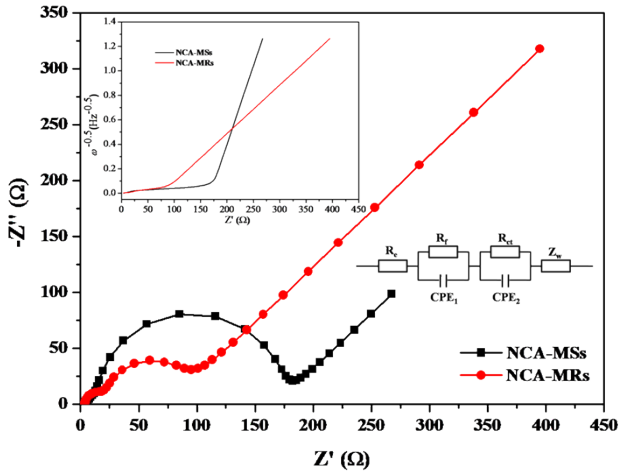

Fig. S9 Nyquist plots of NCA-MRs and NCA-MSs electrodes at a charge state of 4.3V after 100 cycles at 25 ºC under 1C and the equivalent circuit used to fit the measured impedance spectra; top left inset show Z′ vs. $\omega^{-1/2}$

As shown in Fig. S9~~8~~, the two electrodes were carried out with a full charge state of 4.3 V (vs. Li/Li$^+$) after 100 cycles at 25 ^{o}C under 1C, the Nyquist plots for both electrodes are all composed of a semi-circle in the high frequency region and a quasi-straight line in the low frequency region. Generally, the semi-circle in high frequency region is assigned to the charge transfer resistance (R_{ct}) in the electrode/electrolyte interface; the low frequency region of the quasi-straight line is attributed to the Warburg diffusion process of Li ion into the electrode materials.

As summarized in Table S5, the R_e (fitted combined impedance of the electrolyte and cell components) and the R_{SEI} (solid electrolyte interface resistance) of the NCA-MRs are smaller than that of the NCA-MSs, while the R_{ct} at the 100th cycles of the NCA-MRs (59.32 Ω) is much smaller than that of the MSs (156.2 Ω), indicating that the microrod structure can effectively reduce the resistance for Li$^+$ ion transfer at the electrode/electrolyte interface in the cells.

Moreover, the Li$^+$ ion diffusion coefficients calculated from EIS date according to the following equation[S2]:

$$D_{Li}=R^2T^2/2A^2F^4n^4C^2\sigma^2 \quad (1)$$

Where D_{Li} is the diffusion coefficient of Li$^+$ ion, R is the gas constant (R=8.314 J/(mol·K)), T is the absolute temperature (T=298 K), A is the surface area of the positive electrode (A=1.54 cm^2), F is the Faraday's constant (F=96485.33 C/mol), n is the number of transferred

concentration in cathode material, C is the concentration of lithium-ion (C=0.04936 mol/cm^3) and σ is the Warburg factor which is obtained from the slope of Z' vs. Reciprocal square root of the frequency in the low frequency region ($\omega^{-1/2}$). Clearly, the calculated D_{Li} for the NCA-MRs is approximately 10 times larger than that for the NCA-MSs, which demonstrates that the NCA with a rod-like structure can effectively shorten the pathways for Li^+ ion diffusion as compared with the NCA with a spherical structure, thus a remarkable improved electrochemical performances are achieved.

Table S5. The values of R_e, R_{SEI} and R_{ct} for the Nyquist plots and calculated Li^+ ion diffusion coefficient (D_{Li}) for NCA-MSs and NCA-MRs after 100 cycles at 25 °C under 1C

Samples	NCA-MSs	NCA-MRs
R_e(Ω)	5.68	3.49
R_{SEI}(Ω)	7.27	14.53
R_{ct}(Ω)	156.2	59.32
σ	0.01282	0.00397
D_{Li}(cm^2/S)	3.72E-11	3.89E-10

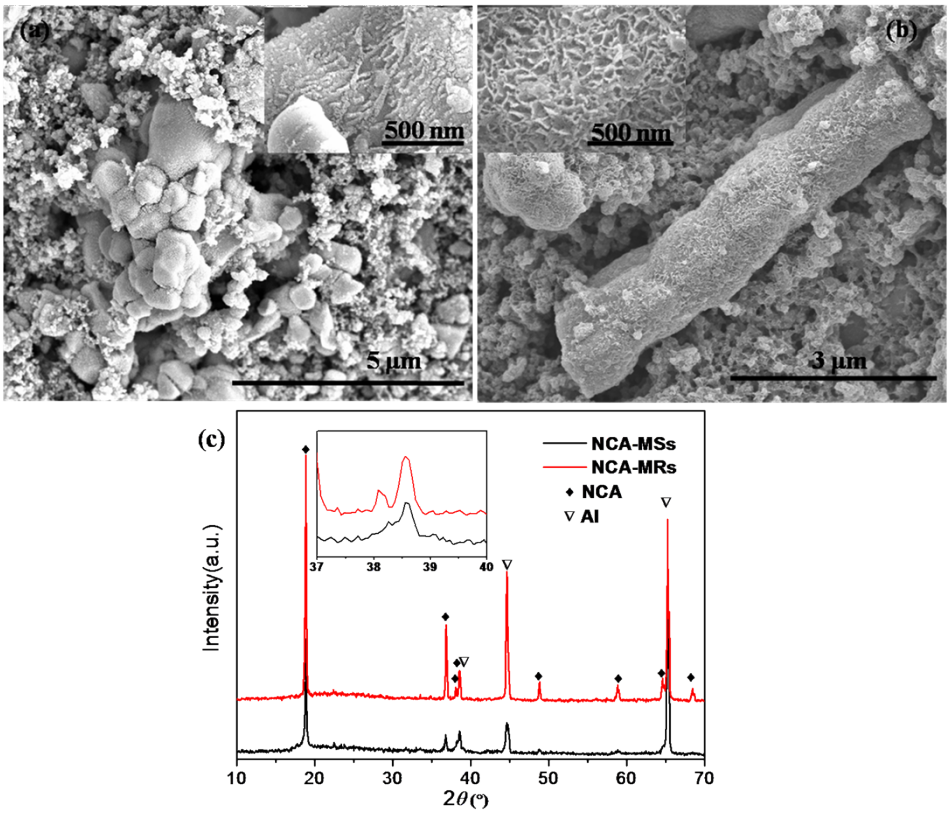

Fig. S10(a), (b) SEM images and (c) XRD patterns of NCA-MSs and NCA-MRs after 100 cycles at 55 °C under 1C (inset: diffraction peaks of the region from 37 to 40°)

References:

S1 C. Fu, G. Li, D. Luo, Q. Li, J. Fan and L. Li, *ACS Appl. Mater. Interfaces,* 2014, **6**, 15822−15831.

S2~~1~~ P. Gao, Y. Li, H. Liua, J. Pinto, X. Jiang and G. Yang, *J. Electrochem. Soc.*, 2012, **159**, A506-A513.